Impact Damage Visualization of Heterogeneous Two-layer Materials Subjected to Low-speed Impact

L. ROY XU*

Department of Civil and Environmental Engineering
Station B 351831, Vanderbilt University
Nashville, TN 37235, USA

ARES J. ROSAKIS

Graduate Aeronautical Laboratories
California Institute of Technology
Pasadena, CA 91125, USA

ABSTRACT: A systematic experimental investigation of the generation and subsequent evolution of impact damage in heterogeneous two-layer materials is presented. Model layered specimens involving a compliant polymer layer bonded with a metal layer were designed and subjected to impact loading to simulate failure mechanisms in real time. High-speed photography and dynamic photoelasticity were utilized to visualize the nature and sequence of dynamic failure modes. A series of complex failure modes was documented. Interlayer crack growth (interfacial delamination) is the dominant dynamic failure mode. These cracks appear to be shear dominated and might proceed with intersonic speeds. Intralayer cracking always occurs in a local Mode I crack inside the weak layer. Both impact speed and interfacial bonding strength have significant influence on the impact failure. High-impact loading leads to high interlayer crack speeds. Specimens featuring ductile and weak bonds subjected to high-impact speeds are shown to feature intersonic cracks with clearly visible shear shock wave (Mach lines) emitted from the crack tips.

KEY WORDS: impact damage, failure visualization, layered materials.

INTRODUCTION

LAYERED MATERIALS AND structures have extensive applications in many areas of engineering. These include the increased use of composite laminates and armor systems used in aerospace and defensive engineering, and the use of thin films/layered structures in microelectronic components (Wu and Springer, 1988; Choi et al., 1991; Hutchinson and Suo, 1992). While failure characteristics of layered materials subjected to static loading have been investigated extensively in the past years, their dynamic counterparts have remained elusive (Sun and Rechak, 1988; Cantwell and Morton, 1991; Abrate, 1994; Gupta and Madhu, 1997; Wen et al., 1998; Mines et al., 1999; Han and Sun, 2000; Vetrovec et al., 2001; Gupta and Ding, 2002). Indeed, the presence of highly complex and transient dynamic failure modes in such materials, and the inaccessibility of internal damage to real-time scruting have resulted in experimental studies limited to the final impact damage characteristics of failure and to the measurement of postmortem properties. To begin addressing the need for real-time observations of failure events, the work presented here focuses on the study of such events in model layered materials, and in particular, on the identification of their nature, chronological evolution, and interaction.

To identify the evolution of failure for different loading regimes, it is convenient to first classify these modes based on the material constitutions of layered/reinforced materials (Xu and Rosakis, 2002a). According to the impact failure observed in postmortem studies, the first major failure category is decohesion (or cracking) between bonded layers at an interface, which is also called interlayer failure. The second major category is referred to as intralayer failure, i.e., failure occurring inside the layer. As stated earlier, for most layered materials, the presence of such highly complicated dynamic failure modes and the inaccessibility of internal damage to direct observation explain the fact that only the final impact damage character-istics of such structures are usually discussed in the open literature. Indeed, the sequence, nature, and interaction of such failure process were never properly clarified. Notable exception to this rule is the early studies of Takeda et al. (1982), who observed the evolution and sequence of matrix cracks and delamination failure in glass fiber composite laminates under ballistic impact. Recently, Riou et al. (1998) visualized the impact damage in a ceramic layer using high-speed photography. Their results were very valuable in understanding the basic failure mechanisms of ceramics/metal armor systems, whose impact damage is quite complicated.

For many complex engineering problems, model experiments may prove extremely useful as intermediate steps, which reveal the basic physics

of the problem and provide relatively straightforward explanations of the failure patterns seen in postmortem observations. A striking example of this approach was provided by Riley and Dally (1966), who designed a model metal–polymer layered system subjected to dynamic loading. Their model configuration was designed to simulate stress waves in layered structures. More recently, Parameswaran et al. (1999) designed and tested two-layer specimens to simulate the ballistic performance of a composite armor. In our experiments, we also adopt the same idea and introduce an appropriate intermediate model configuration. In order to simulate the difficult three-dimensional problem of the out-of-plane impact of layered structures and to simultaneously preserve the essence of the failure phenomena involved, we introduce a two-dimensional plane-stress specimen, which represents a cross-sectional cut of the layered material. For this type of model specimen, the failure process is easy to record, visualize, and analyze. It is noted that although the exact impact mechanics involved in two configurations is not identical (the real case is three-dimensional while the model specimen is closer to a plane stress state), the mechanisms of stress wave propagation and failure progression of the real and the model layered materials are quite analogous. In designing these model two-dimensional sandwich specimens, it is important to obey the similarity rules. Selecting similar Dundurs' parameters (Hutchinson and Suo, 1992) may ensure similarity of the elasto-static response for the interfacial mechanics problem. Meanwhile, selecting model material combinations with similar ratios of wave speeds of two constitution materials to the real structure is perhaps the most important consideration in the dynamic case, where timing of events and stress intensity are governed by the constituent material wave speeds. Also, the ratio of interlayer and intra-layer strengths (or fracture toughnesses) is important. These three issues provide sets of similarity rules to connect the real structures to our model tests.

The objectives of the current work are to conduct systematic experimental studies of the time evolution and nature of different dynamic failure modes, and to investigate their interactions. Through these model experiments, we try to identify the basic physical phenomena, and to provide guidance for theoretical models and much needed, real-time validation of numerical codes. Since the two-layer and the three-layer systems are the two basic configurations for general layered materials or structures, in this investigation, we mainly focus on the impact damage in heterogeneous two-layer systems. Results on the three-layer systems and the homogeneous two-layer systems have been reported by the authors (Xu and Rosakis, 2002a, b, 2003a).

EXPERIMENTAL PROCEDURE

Materials and Specimens

Two kinds of materials were used in the experiments. A 4340-carbon steel was employed to simulate the stiff and strong layer in a general layered material. Homalite-100, a polymeric material, was used to simulate the soft and weak layer. Some physical properties of these model materials are listed in Table 1. Loctite-330 was the major adhesive used to bond the metal–polymer interface. The mechanical properties of this adhesive and the effect of interfacial strength variation on the dynamic failure mode selection were reported by Xu and Rosakis (2002b). A typical two-layer specimen generally contains one metal layer bonded with one polymer layer. The overall dimensions of each bonded specimen are 254 mm (length), 76.2 mm (width), and 6.35 mm (thickness).

Experimental Setup

Most of the experiments in this investigation were performed using dynamic photoelasticity. This classical method has recently found a lot of new applications such as the study of the dynamic fracture processes in functionally gradient materials (FGMs) described by Parameswaran and Shukla (1998). A schematic diagram of the dynamic photoelasticity setup used here is given in Figure 1. Two circular polarizer sheets were placed on either side of the specimen. An Innova Sabre argon-ion pulsed laser was used as the light source. The coherent, monochromatic, plane polarized light output was collimated to a circular beam of 100 mm in diameter. The laser beam was transmitted through the specimen and the resulting fringe pattern was recorded by a high-speed camera. A rotating mirror-type high-speed

Table 1. Material properties used in model experiments.

| Property | Homalite 100 | | Steel 4340 |
	Static	Dynamic*	Static
Young's modulus E (GPa)	3.9	5.3	208
Poisson's ratio ν	0.35	0.35	0.3
Dilatational wave speed c_l (m/s) (plane stress)	1890	2119	5500
Shear wave speed c_s (m/s)	1080	1208	3320
Rayleigh wave speed c_r (m/s)	1010	1110	2950
Density ρ (kg/m^3)	1230	1230	7830

*Dynamic properties correspond to an average equivalent strain rate of 10^3/s.
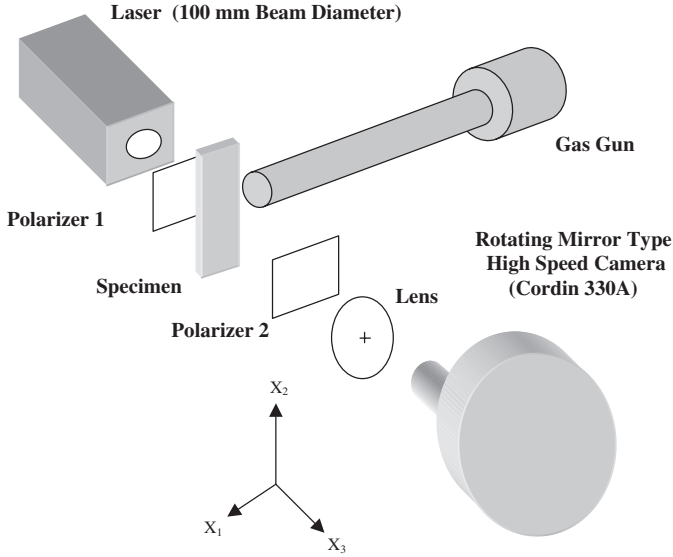
Figure 1. Schematic diagram of the dynamic photoelasticity setup.

film camera was used to record the images. During the impact test, a projectile was fired by a gas gun and impacted the specimen center. The generation of isochromatic fringe patterns is governed by the stress-optic law. In the case of monochromatic light, the condition for the formation of fringes can be expressed as (Dally, 1979):

$$\hat{\sigma}_1 - \hat{\sigma}_2 = \frac{N f_\sigma}{h}$$

where $\hat{\sigma}_1 - \hat{\sigma}_2$ is the principal stress difference of the thickness-averaged stress tensor. f_σ is the material fringe value, N is the isochromatic fringe order, and h is the specimen thickness. The isochromatic fringe patterns observed are proportional to contours of constant maximum in-plane shear stress, $\hat{\tau}_{\max} = (\hat{\sigma}_1 - \hat{\sigma}_2)/2$.

RESULTS AND DISCUSSION

Impact Damage Visualization of A Baseline Two-layer Specimen

In this investigation, we designed and tested a baseline two-layer specimen at first. Then, influences of impact speeds, interfacial bonding strengths, and other factors were explored for comparison. As shown in Figure 2, the
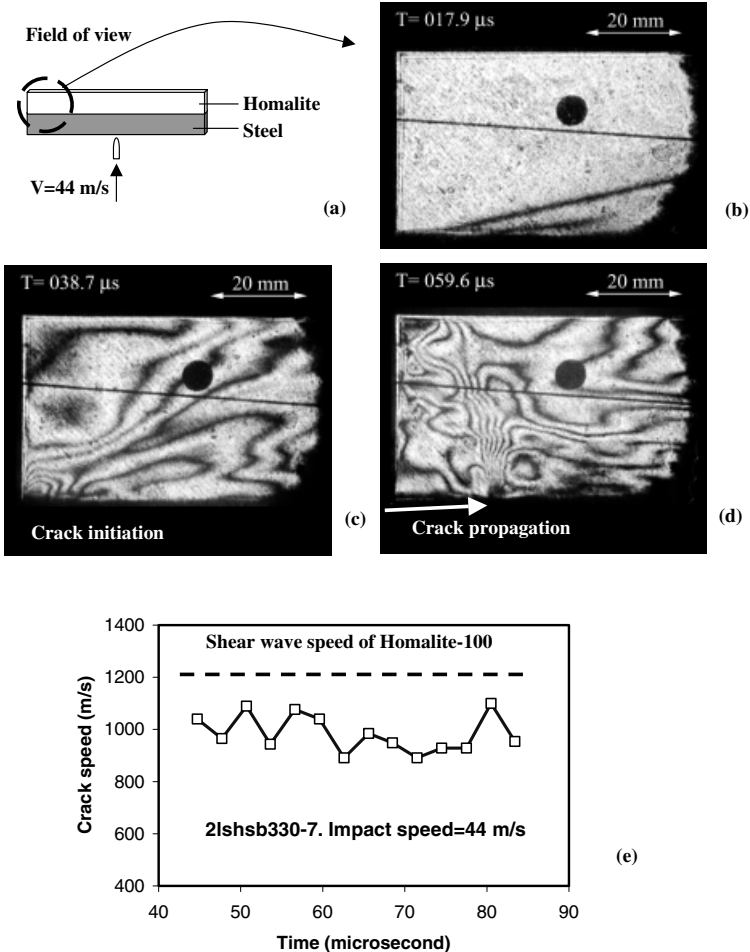
Figure 2. Interlayer crack initiation and propagation in a baseline two-layer specimen (b)–(d), and crack speed history (e).

impact speed for the baseline case was 44 m/s. In all the experiments, the projectile impacted the center of the bottom metal layer. Since the diameter of the laser beam used in this investigation was 100 mm, and the maximum length of the zone that had to be investigated was 254 mm, in order to observe all possible dynamic failure modes, the field of view had to be moved from one location to another for each specimen configuration under the same impact condition. Figure 2 presents a series of photoelastic images of the Homalite layer with a field of view at the specimen edge. The dark circular spot at the upper right corner is a scaling mark (diameter 6.35 mm)

bonded on the specimen. A thin horizontal dark line, seen around the center of every image, is the streak line of the camera. This line provides a stationary reference when the whole specimen moves during the impact process.

As shown in Figure 2(b), after impact at the specimen center, the stress waves in the bottom steel layer propagates toward the edge creating a visible head wave structure on the lower wave speed polymer side. Right after the stress wave reaches the free edge, due to the existence of a stress singularity at the bimaterial corner (Williams, 1952; Bogy, 1971), an interlayer crack initiates at the lower interface around 39 µs after impact, as seen in Figure 2(c). This crack propagates toward the specimen center, identified by a moving concentration of fringes at its tip, as seen in Figure 2(d). Similar to the shear dominated interfacial cracks in bimaterials (Lambros and Rosakis, 1995; Singh and Shukla, 1996), these interlayer cracks are also shear dominated. Since the Homalite and steel layers are still in contact at that time, no visual evidence of decohesion is apparent in the images, although these cracks have already broken the interface in a combination of compression and shear. The crack speed history for the interlayer crack is plotted in Figure 2(e). The dynamic shear wave speed of Homalite-100 (see Table 1) is also shown as a horizontal dashed line. This value has been obtained experimentally by the procedure outlined by Xu and Rosakis (2003a).

In order to investigate a complete impact damage process of the whole specimen, the field of view was moved to the specimen center as shown in Figure 3 while a same impact speed was employed. As seen in Figure 3(b) and (c), complicated stress wave propagation and interaction with the upper free edge were observed. In Figure 3(d), two intralayer cracks appear at the interface and propagate toward the upper free edge of the Homalite layer at 69 µs after impact. At a later time, an interlayer crack originating from the free edge as seen in Figure 2 also entered the field of view while two intralayer cracks were propagating toward the upper edge (Figure 3(e)). In Figure 3(f), two rather than one interlayer cracks are observed at the specimen center but two intralayer cracks almost reached the upper edge of the Homalite layer. These two experiments, as shown in Figures 2 and 3, formed a baseline impact failure process of a heterogeneous two-layer material. In other experiments, we changed some selected parameters such as impact speed and interfacial strength to understand their influence on the basic failure pattern or sequence.

Influence of Impact Speed

Recently, Needleman and Rosakis (1999), and Xu and Rosakis (2002b) showed that if the impact speed or pulse duration was altered, significant
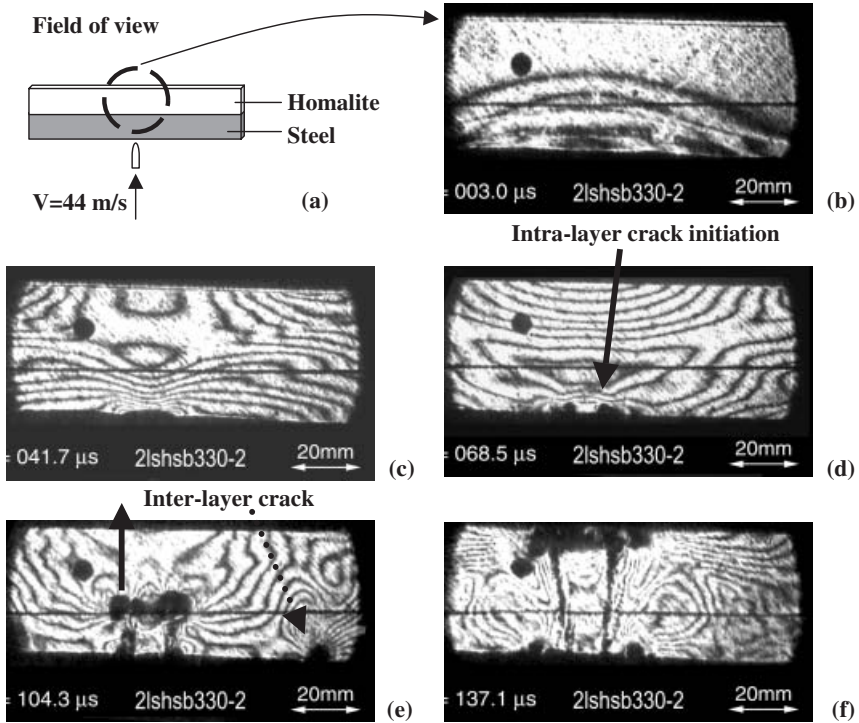
Figure 3. *Two major impact failure modes and sequences observed from a baseline two-layer specimen with a central field of view. Two intralayer cracks initiated from the interface (d) and propagated toward the upper free edge of the Homalite layer (e) while two interlayer cracks entered the central part of the specimen from the left and right edges of the specimen (e) and (f).*

interfacial crack speed variations were observed in bimaterial and layered systems. In this investigation, the baseline impact speed was 44–45 m/s. This impact speed was intentionally reduced and a series of different failure sequences with the baseline failure sequence was revealed.

At first, the impact speed was reduced to 39 m/s for the identical specimens shown in Figures 2 and 3. It is interesting to note that the intralayer crack initiated from the upper free edge rather than from the interface, and propagated toward the interface as shown in Figure 4(b) and (c). The intralayer crack initiated around 128 μs after impact, quite later than 69 μs for the intralayer crack initiation of the baseline specimen as seen in Figure 3(d). Both the intralayer cracks in the two different experiments were Mode I cracks because of their symmetrical fringe patterns and large caustics as seen at the crack tips. It should be noticed that the initiation mechanisms are different for these two cases. The intralayer crack initiation
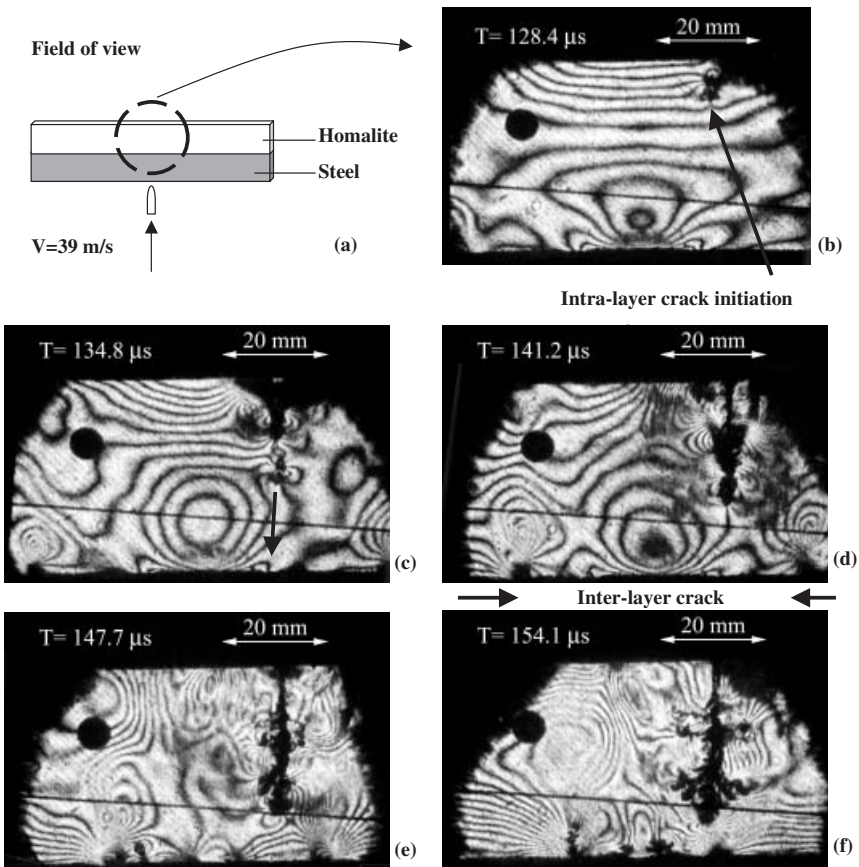
Figure 4. Intralayer crack initiated from the upper free edge and propagated toward the interface (b) and (c). Two interlayer cracks also entered the field of view (c)–(e) and three cracks met at the center of the specimen (f).

from the interface for a higher impact speed case (baseline case) was caused by high local contact stress at the impact site, which was similar to the intralayer crack initiation and propagation in homogenous layered materials (Xu and Rosakis, 2003a). The intralayer crack initiation in Figure 4(b) is due to the high tensile stress at the upper free edge caused by stress wave transition. Similarly, in Figure 4(c)–(e), two interlayer cracks enter the field of view and propagate toward the specimen center. Thereafter, very complicated fringe patterns can be observed in Figure 4(f) since two interlayer cracks and one intralayer crack meet at the specimen center. A significant crack branching phenomenon was observed because the

intralayer crack speed exceeded 30–40% of the shear wave speed of Homalite-100, which led to a dynamic crack branching (Xu and Rosakis, 2003b).

If the impact speed was reduced to a low value, i.e., 14 m/s, the above failure pattern and sequence were significantly changed. In the above two cases of relatively high impact speeds, two interlayer cracks initiated from the left/right bimaterial edges with stress singularities, reached the specimen center at 140–150 μs after impact. Due to the lower impact speed, the induced stress wave might be not strong enough to lead to edge interfacial debonding in this case. However, higher interfacial shear stress beside the impact site as predicted by finite element analysis (Xu and Rosakis, 2002a) also led to interfacial debonding as shown in Figure 5(b) and (c). This interlayer crack propagated toward the right and left free edges while its speed varied significantly. It almost arrested at 160 μs because of the complicated stress wave interaction, and soon it kinked into the Homalite layer as seen in Figure 5(g) and (h). The crack extension and speed history is plotted in Figure 6(a) and (b) for the left interlayer crack tip. Surprisingly, we find that the crack speed varied from 900 to 300 m/s. A similar phenomenon of dynamic crack initiation, propagation, and arrest was also observed in the heterogeneous three-layer systems (Xu and Rosakis, 2002a).

In summary, the influence of impact speed on the impact failure patterns and sequences is illustrated in Figure 7. Figure 7(a) and (b) represent the interlayer crack initiation and propagation, and transition (or kinking) into the intralayer crack for the very low impact speed case (14 m/s). However, such kind of failure sequence is totally altered if the impact speed is increased to 39 m/s. For relatively high impact speed, reflected tensile stress wave induced interfacial debonding at the right and left edges with intrinsic stress singularities (Figure 7(c)). Meanwhile, reflected tensile stress wave is strong enough to induce an intralayer crack from the upper free edge. Three cracks are expected to meet in the middle of the specimen (Figure 7(d)). If the impact speed is increased to 44–45 m/s, interlayer cracks appear from the right and left free edges again, but two intralayer cracks initiate from the interface and propagate toward the upper free edge (Figure 7(e)). These two intralayer cracks are caused by high local contact stress due to the high-speed projectile. In terms of mechanics nature, all these intralayer cracks are opening (Mode I) cracks and all interlayer cracks are shear dominated interfacial cracks.

Effect of Interfacial Strengths

In order to compare the effect of different interfacial bond strengths on impact failure in layered materials, three different kinds of adhesives were used to construct interfacial bonds of various strengths. The bond strengths
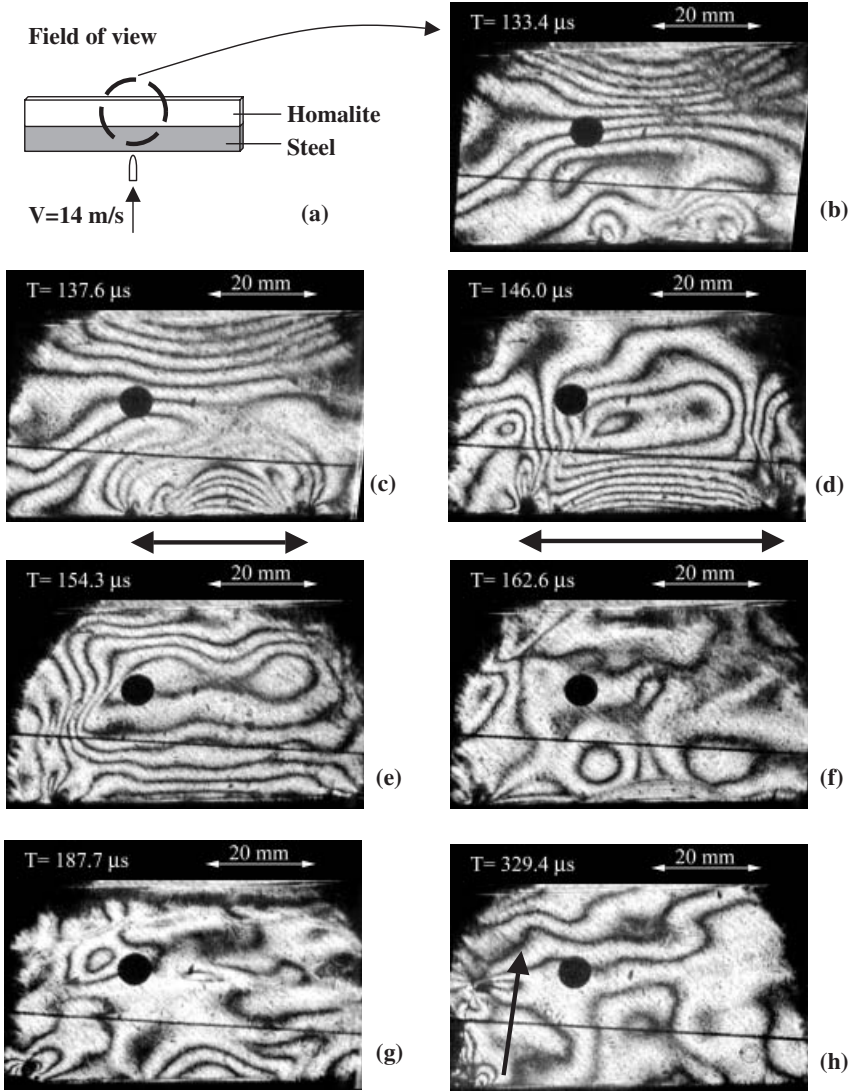
Figure 5. *Interlayer crack initiated in the middle of the specimen and propagated toward two edges (b)–(e). This interlayer crack met another interlayer crack initiated from the edge of the specimen (code 2lshsb330-6) and an intralayer crack formed in (g) and (h).*

for Homalite–adhesive–Homalite interfaces have been reported by the authors (Xu and Rosakis, 2002b). Owing to the stress singularity at bimaterial corners, it is hard to obtain the intrinsic bonding properties of bimaterial interfaces based on current specimen configurations (Xu and
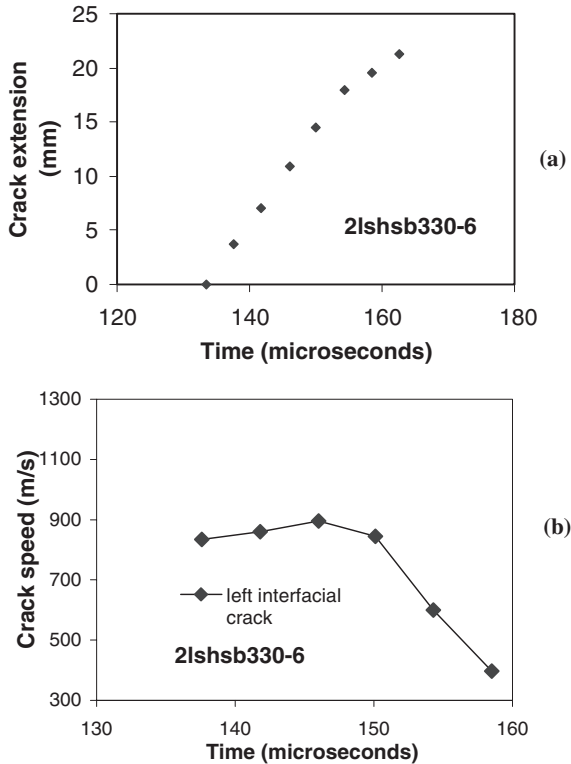
Figure 6. Crack length history (a) and crack speed history (b) for the interlayer crack shown in Figure 5 (measured from the left crack tip).

Rosakis, 2002b). Instead in Table 1, we only list the strengths of these adhesives when they are used to bond identical Homalite pieces. This is done to provide relative levels of strengths of these adhesives. The Weldon-10 and Loctite 330 are considered to be 'strong' adhesives because these two kinds of adhesives have quite high nominal tensile strengths (Xu and Rosakis, 2002b). However, the interfacial shear strength of Weldon-10 is much higher than that of Loctite 330. Loctite 5083 gives a weak and ductile bond because its elongation at failure in cured bulk form is as high as 170%. The average thickness of the adhesive layer is less than 20 μm. Here, in order to investigate the relative effect of various interfacial bond strengths, the base-line specimen configuration is chosen as the one shown in Figures 2 and 3, which features the Loctite-330 strong bonding and is subjected to an impact speed of 45 m/s.

Figure 8 shows a sequence of images of two specimens featuring the strong and weak bonds, but the same impact condition with the baseline
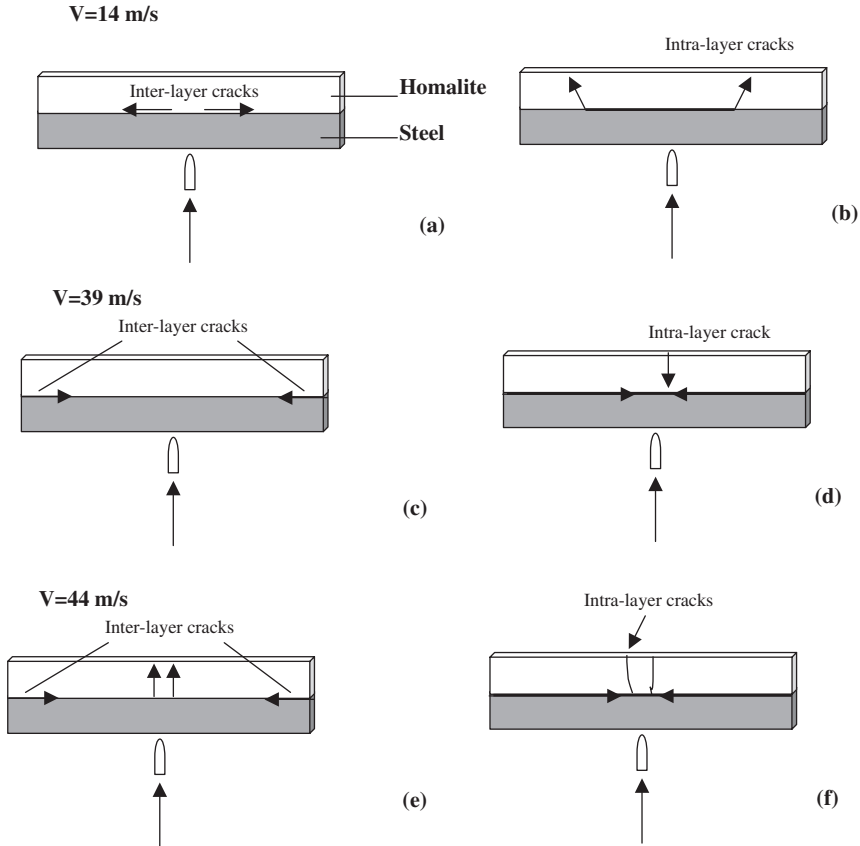
V=14 m/s

Inter-layer cracks

Homalite

Steel

Intra-layer cracks

(a)

(b)

V=39 m/s

Inter-layer cracks

Intra-layer crack

(c)

(d)

V=44 m/s

Inter-layer cracks

Intra-layer cracks

(e)

(f)

Figure 7. A summary of influence of impact speeds on the impact failure modes and sequence of a two-layer specimen impacted on the strong layer.

specimen. The failure characteristics of the specimen featuring the strong Weldon-10 bond (Figure 8(b) and (c)) are quite similar to the ones observed in the baseline specimen featuring the Loctite-330 bond. For example, the interlayer cracks initiated at approximately 40 μs after impact in both the cases. However, for the specimen featuring weak and ductile Loctite 5083 bond, as shown in Figure 8(d)–(f), an interlayer crack generated at the specimen edge around 106 μs after impact, much later than the previous case. Also, a thin shear shock line inclined at an angle slightly above 45° to the horizontal interface (Figure 8(f)) marks the position of this crack which clearly moves intersonically to the right. Since the 5083 bond strength is very low, the stress/fringe concentration of the moving crack tip appears less strong than in the baseline case (see Figure 2). As shown in Figure 9, the
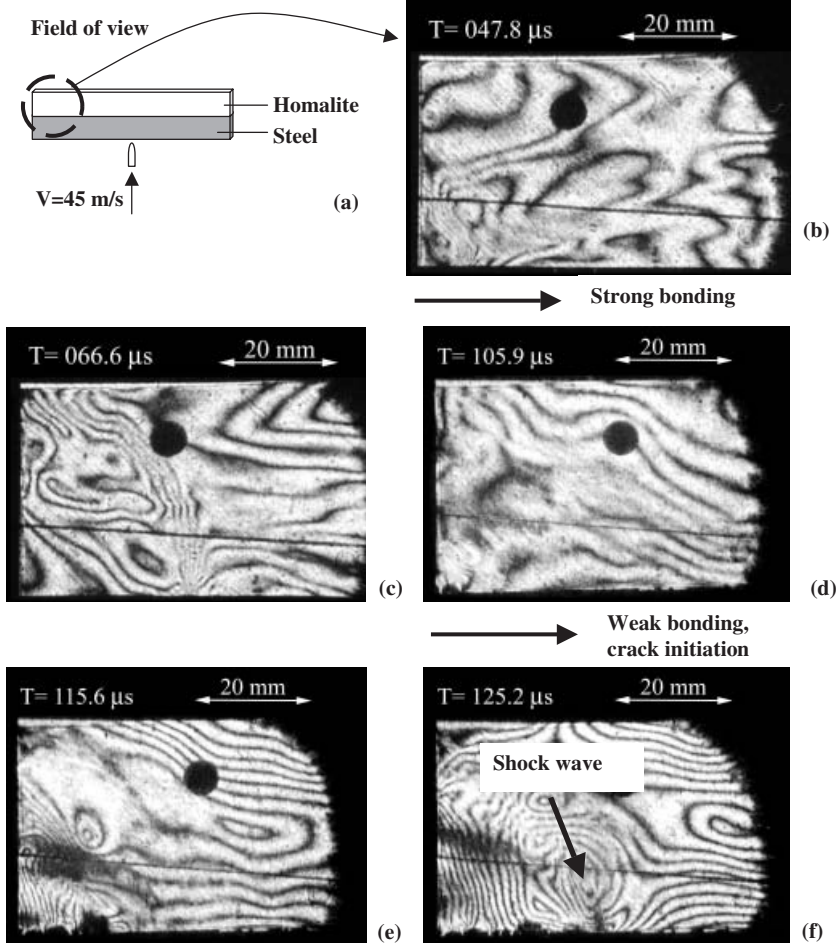
Figure 8. Influence of interfacial strength on the impact failure (b) and (c) for specimen 2lshsbwd-5 featuring strong Weldon-10 bonding (d)–(f) for specimen 2lshsb5083-2 featuring Loctite 5083 weak and ductile bonding.

crack tip speed in this case, however, is very much higher than that in other cases and, at the initial stages, is close to $\sqrt{2}C_s$. To illustrate the significant difference in the crack initiation time and the crack tip speed history between the otherwise identical specimens featuring strong and weak bonds, let us compare Figure 9 and Figure 2(e). In both the cases, the field of view was concentrated at the specimen edges. It is observed that the weak but ductile 5083 adhesive results in longer initiation time and very high crack tip speeds. These speeds were initially close to $\sqrt{2}C_s$ then decreased to C_s as the
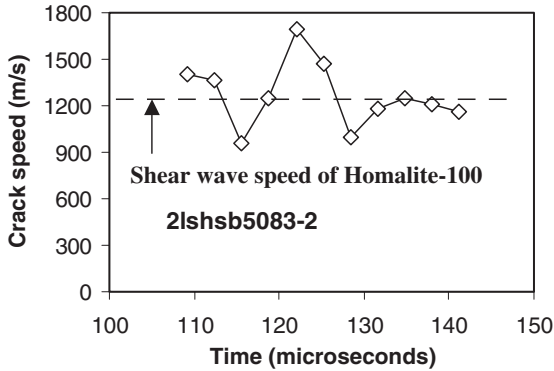
Figure 9. *Crack tip speed history of the specimen featuring Loctite 5083 weak and ductile bonding. The horizontal line is the shear wave speed of Homalite layer.*

specimen center is approached. On the other hand, the strong Loctite-330 bond features a short initiation time and more moderate crack speeds ranging from the Rayleigh wave speed to just above the shear wave speed.

Direct Impact on the Brittle Polymeric Layer

All above the experiments were focused on the impact on the strong steel layer. However, in some applications of layered materials, direct impact on the brittle layer such as ceramics layer in composite armor is also very important since their failure behavior might be very different. Selected experiments were conducted on direct impact on the brittle polymer layer. As shown in Figure 10, a complicated stress wave propagation, projectile penetration, and large deformation process was observed for a two-layer system with a weak and ductile 5083 bond. As soon as the projectile impacted the transparent Homalite layer, a series of fringe patterns related to stress waves developed around the impact site. The projectile head kept moving and complicated stress wave interaction and propagation were observed around 10 μs after impact (Figure 10(b) and (c)). It should be noticed that the movement of the projectile was not obvious. In the next stage of projectile penetration, a black contact zone was observed at the impact site and an intralayer crack initiated and propagated toward the interface. In Figure 10(f), it seems that this intralayer crack arrests at the interface since no significant interfacial crack propagation (moving fringe concentration) was observed in the images that followed. As discussed by Xu and Rosakis (2003a), the crack arrest mechanism by a ductile and weak adhesive layer is due to the dramatical stress wave gradient change across
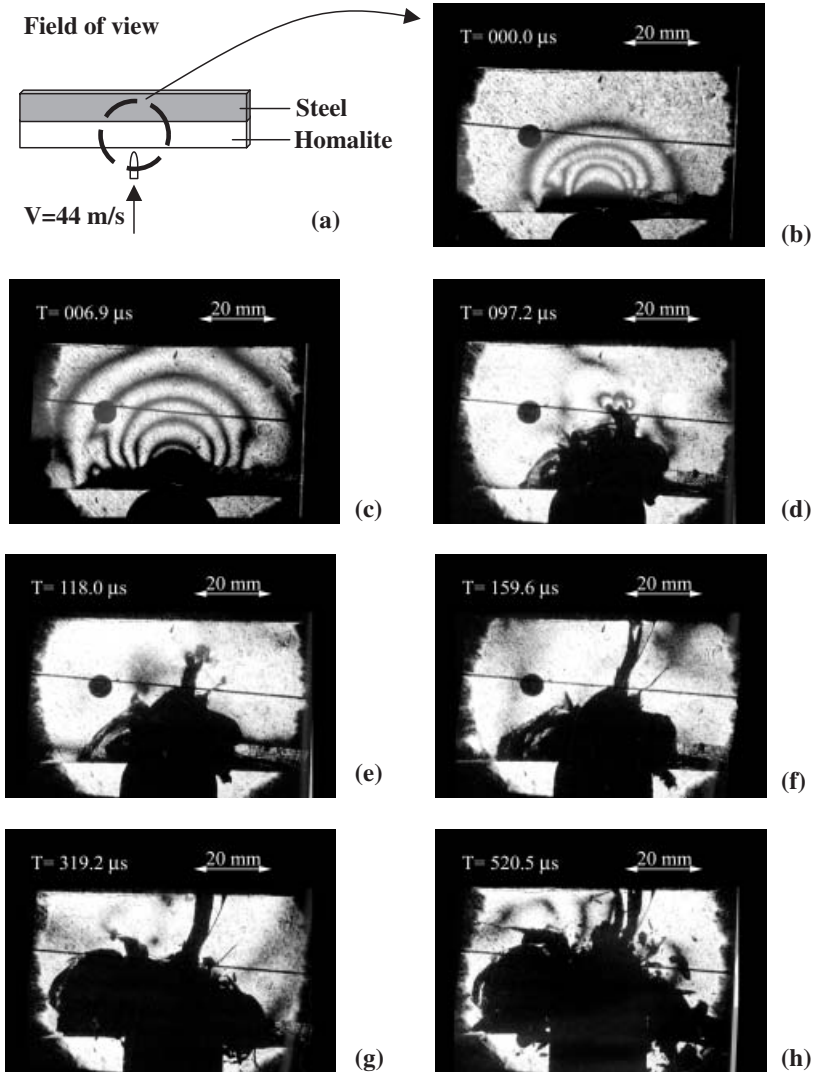
Figure 10. *Failure sequence of a two-layer specimen impacted directly on the brittle Homalite layer (b) and (c) show a complicated stress wave process, (d)–(f) reveal intralayer crack initiation and propagation while (g) and (h) demonstrate a penetration procedure with large local deformation.*

the adhesive layer. After 300 μs of impact (Figure 10(g)–(h)), a large contact zone appeared in a growing black zone connected to the projectile. Owing to the large deformation inside the contact zone, those transmitted laser rays were deflected and cannot enter the camera and hence only a black zone was

recorded. Meanwhile, some materials were flying out from the Homalite layer because of the fragments of brittle Homalite subjected to high contact force. Compared to the impact on the strong steel layer of previous cases, direct impact on the brittle Homalite layer has more severe damage in the local impact site.

Long Specimens and General Multilayered Materials

In order to extend our observation to a more general situation, selected two-, four-, and five-layer specimens with doubled lengths (508 mm) were designed and tested. The purpose of long specimens is to reduce the free-edge effect so that the interfacial crack initiates from locations close to the impact side rather than the specimen edges (Xu and Rosakis, 2002a). We found that the intralayer crack initiated at the interface and propagated toward the upper free interface for a long specimen featuring Weldon-10 strong bonding around 70 μs after impact (projectile speed is 24 m/s). This process is very similar to that of the short specimen showed in Figure 3 featuring strong Loctite 330 bonding. This is probably because the intralayer cracks initiated from the interface are directly related to the very high local normal stress caused by the projectile impact.

Also, long specimens (508 mm) consisting of four to five layers featuring Weldon-10 strong bonding were designed and impacted at various speeds. It is noticed that the impact failure pattern of multilayered specimens is indeed a combination of the failure patterns of two-layered (reported here) and three-layered specimens (Xu and Rosakis, 2002a). For example, for a four-layered specimen with a direct impact at the metal layer, a similar intralayer crack initiating from the upper free edge of the polymer layer was observed. This failure feature was recorded in Figure 4 for a two-layered specimen, not in a three-layer specimen as discussed by Xu and Rosakis (2002a).

CONCLUDING REMARKS

For heterogeneous two-layer materials subjected to low-speed impact, interlayer crack growth (interfacial delamination) is the dominant dynamic failure mode. These cracks appear to be shear dominated and might proceed with intersonic speeds. Intralayer cracking always occurs in a local Mode I crack inside the weak layer. Both the impact speed and the interfacial bonding strength have profound influences on the impact failure sequence. Specimens with ductile and weak bonds subjected to high-impact speeds are shown to feature intersonic cracks accompanied by the formation of clearly visible shear shock waves (Mach lines) emitted from the crack tips.

ACKNOWLEDGMENTS

REFERENCES

Abrate, S. (1994). Impact on Laminated Composites: Recent Advances, *Applied Mechanics Reviews*, **47**: 517–544.

Bogy, D.B. (1971). Two Edge-bonded Elastic Wedge of Different Materials and Wedge Angles Under Surface Traction, *J. Applied Mechanics*, **38**: 377–386.

Cantwell, W.J. and Morton, J. (1991). The Impact Resistance of Composite Materials—A Review. *Composites*, **22**: 347–362.

Choi, H.Y., Wu, H.T. and Chang, F.-K. (1991). A New Approach Toward Understanding Damage Mechanisms and Mechanics of Laminated Composites Due to Low-velocity Impact: Part II—analysis, *J. Composite Materials*, **25**: 1012–1038.

Dally, J.W. (1979). Dynamic Photoelastic Studies of Fracture, *Experimental Mechanics*, **19**: 349–61.

Gupta, N.K. and Madhu, V. (1997). An Experimental Study of Normal and Oblique Impact of Hard-core Projectile on Single and Layered Plates, *International Journal of Impact Engineering*, **19**: 395–414

Gupta, Y.M. and Ding, J.L. (2002). Impact Load Spreading in Layered Materials and Structures: Concept and Quantitative Measure, *International Journal of Impact Engineering*, **27**: 277–291.

Han, C. and Sun, C.T. (2000). A Study of Pre-stress Effect on Static and Dynamic Contact Failure of Brittle Materials, *International Journal of Impact Engineering*, **24**: 597–611.

Hutchinson, J.W. and Suo, Z. (1992). Mixed Mode Cracking in Layered Materials, *Advances in Applied Mechanics*, **29**: 63–191.

Lambros, J. and Rosakis, A.J. (1995). Shear Dominated Transonic Growth in a Bimaterial –I. Experimental Observations, *J. Mech. Phys. Solids*, **43**: 169–188.

Mines, R.A.W., Roach, A.M. and Jones, N. (1999). High Velocity Perforation Behaviour of Polymer Composite Laminates, *International Journal of Impact Engineering*, **22**: 561–588.

Needleman, A. and Rosakis, A.J. (1999). The Effect of Bond Strength and Loading Rate on the Conditions Governing the Attainment of Intersonic Crack Growth Along Interfaces, *J. Mech. Phys. Solids*, **47**: 2411–2449.

Parameswaran, V. and Shukla, A. (1998). Dynamic Fracture of a Functionally Gradient Material have Discrete Property Variation, *J. Material Science*, **33**: 3303–3311.

Parameswaran, V., Brentley, W., Shukla, A. and Prosser, R.A. (1999). A Bew Approach for Improving Ballistic Performance of Composite Armor, *Experimental Mechanics*, **39**: 103–110.

Riou, P., Denoual, Christophe and Cottenot, Charles E. (1998). Visualization of the Damage Evolution in Impacted Silicon Carbide Ceramics, *International Journal of Impact Engineering*, **21**: 225–235.

Riley, W.F. and Dally, J.W. (1966). A Photoelastic Analysis of Stress Wave Propagation in a Layered Model, *Geophysics*, **31**: 881–99.

Singh, R.P. and Shukla, A. (1996). Subsonic and Intersonic Crack Growth Along a Bimaterial Surface, *Journal of Applied Mechanics*, **63**: 919–924.

Sun, C.T. and Rechak, S. (1988). Effect of adhesive layers on impact damage in composite laminates. In: Whitcomb J.D., editor. Composite materials: testing and design (eighth conference). ASTM STP 972, *American Society for Testing and Materials*, Philadelphia, pp. 97–123.

Takeda, N., Sierakowski, R.L., Ross, C.A. and Malvern, L.E. (1982). Delamination-crack propagation in ballistically impacted glass/epoxy composite laminates. *Experimental Mechanics*, **22**: 19–65.

Vetrovec, J., Padfield, Rees, Schwab, Daniel, Nebolsine, Peter, Hayami, Richard, Zwiener, Mark, Huntington, John and Steven, L. (2001). Hancock Analysis and Testing of Rod-like Penetrators in the 4–5 km/s Velocity Regime, *International Journal of Impact Engineering*, **26**: 797–808.

Wen, H.M., Reddy, T.Y., Reid, S.R. and Soden, P.D. (1998). Indentation, Penetration and Perforation of Composite Laminates and Sandwich Panels Under Quasi-Static and Projectile Loading, *Key Engineering Materials*, **141**–**143**, 501–552.

Williams, M.L. (1952). Stress Singularities Resulting from Various Boundary Conditions in Angular Corners in Extension, *J. Applied Mechanics*, **19**: 526–528.

Wu, H.T. and Springer, G.S. (1988). Measurements of Matrix Cracking and Delamination Caused by Impacted on Composite Plates, *J. Composite Materials*, **22**: 518–532.

Xu, L.R. and Rosakis, A.J. (2002a). Impact Failure Characteristics of Sandwich Structures; Part II: Effects of Impact Speeds and Interfacial Bonding Strengths, *International Journal of Solids and Structures*, **39**: 4215–35.

Xu, L.R. and Rosakis, A.J. (2002b). Impact Failure Characteristics in Sandwich Structures; Part II: Effects of Impact Speed and Interfacial Strength, *International Journal of Solids and Structures*, **39**: 4237–48.

Xu, L.R. and Rosakis, A.J. (2003a). An Experimental Study on Impact-induced Failure Events in Homogeneous Layered Materials Using Dynamic Photoelasticity and High-speed Photography, *Optics and Lasers in Engineering*, **40**: 263–288.

Xu, L.R. and Rosakis, A.J. (2003b). Real-time Experimental Investigation of Dynamic Crack Branching Using High-speed Optical Diagnostics, *SEM Experimental Techniques*, **27**: 23–26.